A phantom for simplified image quality control of dental cone beam computed tomography units

Torgersen, Gerald R.; Hol, Caroline; Moystad, Anne; Hellen-Halme, Kristina; Nilsson, Mats

Published in:
Oral Surgery, Oral Medicine, Oral Pathology and Oral Radiology

DOI:
10.1016/j.oooo.2014.08.003

2014

A phantom for simplified image quality control of dental cone beam computed tomography units

Gerald R. Torgersen, MSc,[a] Caroline Hol, DDS,[b] Anne Møystad, DDS, DrOdont,[a] Kristina Hellén-Halme, DDS, OdontDr,[c] and Mats Nilsson, PhD[c,d]

University of Oslo, Oslo, Norway; Competence Centre of the Dental Health Service Region South, Arendal, Norway; Malmö University, Malmö, Sweden; Skåne University Hospital, Malmö, Sweden

Objective. The purpose of this work was to develop an inexpensive phantom for simplified image quality assurance (IQA) together with algorithms for objective evaluation of image quality parameters and to integrate these components into an easy-to-use software package. This should help make quality control of dental cone beam computed tomography (CBCT) units accessible, easy, and affordable for any specialist or general practitioner.

Study Design. Our study developed an inexpensive polymethyl methacrylate (Plexiglas) phantom containing objects and structures for objective quantification of the most important image-quality parameters in CBCT imaging. It also paired the phantom with a software package, based on open-source software, for automatic processing and analysis.

Results. The software produces objectively measured IQA data for low- and high-contrast resolution, uniformity, noise characteristics, and geometric linearity.

Conclusions. The authors consider the phantom and methods presented in this article to be a step toward helping clinical dental personnel perform regular quality assurance on CBCT units. (Oral Surg Oral Med Oral Pathol Oral Radiol 2014;118: 603-611)

Dental cone beam computed tomography (CBCT) has been used in dental radiography for more than 10 years and has been widely available for both specialists and general dental practitioners in most developed countries. In recent years, the use of CBCT has grown rapidly, especially in the fields of implant dentistry, orthodontic treatment, and endodontic treatment. Major concerns have been raised regarding the indications for use of CBCT because of the radiation doses that patients receive. A multinational task group ("Sedentexct") was set up within the Seventh Framework Programme of the European Atomic Energy Community (Euratom) to systematically analyze the evidence regarding the application of CBCT in clinical situations and to publish guidelines for its proper use.[1] Quality assurance (QA) of CBCT units is a particularly important issue addressed in the guidelines.

QA procedures can be divided into 2 groups: Dosimetric QA and image QA (IQA). Dosimetric QA should be carried out by a medical physics expert or clinical engineer using properly calibrated equipment, whereas IQA should preferably be done by clinical workers: Dentists, dental nurses, or hygienists. IQA should also be carried out more frequently than dosimetric QA; monthly IQA should be considered good practice. In addition, software upgrades demand additional IQA.

QA methods in radiology, especially medical radiology, have traditionally been developed by physicists and engineers. To carry out QA, medical radiology departments have engaged physicists and engineers, some as department employees, others as consultants from dedicated service companies, or service personnel from the manufacturers or vendors. In dental radiology, however, this has not been the case. QA procedures have generally been performed by service engineers from the vendors and, up to now, have focused on intraoral and, to some extent, panoramic equipment. The service organizations of the vendors are not suited to the task of doing QA, especially IQA, at the level and frequency that high-quality CBCT requires.[1,2]

Furthermore, evaluation of image quality using commercially available phantoms (e.g., those from QRM

Statement of Clinical Relevance

Image quality assurance for cone beam computed tomography procedures is essential for maintaining good diagnostic accuracy. It is important that the clinical personnel are engaged in performing tests on a regular basis, using easy and understandable procedures.

Presented as a poster at the 19th Congress of the International Association of Dento-Maxillo-Facial Radiology (IADMFR), Bergen, Norway, 2013.

[a]Department of Maxillofacial Radiology, Institute of Clinical Odontology, Faculty of Dentistry, University of Oslo.

[b]Competence Centre of the Dental Health Service Region South, Arendal, Norway.

[c]Department of Oral and Maxillofacial Radiology, Faculty of Odontology, Malmö University.

[d]Department of Radiation Physics, Skåne University Hospital.

Received for publication Mar 26, 2014; returned for revision Jul 21, 2014; accepted for publication Aug 6, 2014.

2212-4403/$ - see front matter

http://dx.doi.org/10.1016/j.oooo.2014.08.003

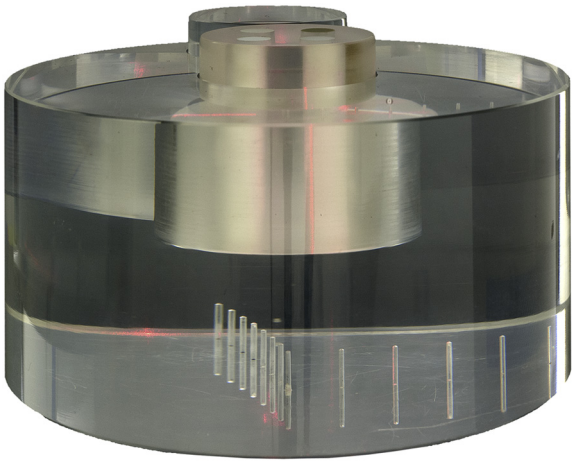

Fig. 1. Photograph of the phantom.

GmbH or Leeds Test Objects Ltd) depends, to a great extent, on methods requiring subjective evaluations. In our opinion, we need objective evaluation methods for IQA. These methods, which must be used frequently by clinical personnel, should be very easy to perform and must not be time-consuming. Ideally, they should be operated without user input and produce results that are easily understandable, such as "passed" or "failed." To set action levels for production of such binary results requires a vast amount of measured data as input and a thorough analysis of diagnostic outcome when data for the measured parameters are impaired. Therefore, time and experience are needed to propose action levels for the parameters studied in the IQA. Additionally, to be accepted by general practitioners, equipment that the clinic must purchase for IQA must not be too expensive. In a recent publication,[3] a phantom and dedicated software for IQA were presented. That publication also promoted measurement of the same IQA parameters as used in this article, with the difference that measurement of spatial resolution is made also in the Z direction using an edge spread function and that a hole pattern for subjective evaluation of the spatial resolution limit also is used. At this stage, the simplified method described in this article does not quantify the spatial resolution in the Z direction. However, their phantom, also constructed for objective measurements, is highly sophisticated and is intended for use by physicists and engineers. Furthermore, the minimum field size for IQA with their proposed procedures is 10 × 10 cm. We believe that simple IQA using smaller field sizes is even more important. Ideally, it should be possible to acquire in 1 scan all of the IQA parameters needed to describe the status of the unit, even for the smallest field of view used.

In the era of analog imaging, IQA methods relied on imaging of phantoms followed by subjective evaluation of the quality parameters using the x-ray film and a light box. Even for the intrinsic digital modalities, such as CT, hardcopies from a laser printer were viewed on a light box for QA purposes. Subjective evaluation, however, has major drawbacks and many confounding factors that inevitably will affect the results obtained. Surprisingly, the use of images of QA phantoms that require subjective evaluation has persisted for many years in the field of digital imaging. An important step toward improved IQA methods is therefore to replace subjective evaluation with objective measurements that directly make use of the digital image data.

Thus, the aim of this work was to develop an inexpensive phantom for IQA together with algorithms for consistent, objective evaluation of image quality parameters and to integrate these components into an easy-to-use software package. This equipment will help make quality control of dental CBCT units easy and affordable.

MATERIAL AND METHODS

QA phantom

The phantom was constructed for the purpose of measuring a subset of the IQA parameters that are normally measured by medical physics experts or clinical engineers when doing IQA for medical computed tomography (CT) units or for CBCT units for angiography, radiotherapy, or odontology. From long experience of medical CT QA, the parameters chosen are those that are most important to measure, and the combined result will certainly reflect the condition of the CBCT unit. The IQA procedures chosen are uniformity, noise, contrast linearity, geometric accuracy, low-contrast resolution, and spatial resolution. As suggested by Baek and Pelc,[4] the noise power spectrum is also produced.

The main body of the phantom consists of a polymethyl methacrylate (Plexiglas) cylinder with a diameter of 160 mm (to mimic the x-ray attenuation of a human head) and a height of 70 mm. Two cylindrical cavities, each with a diameter of 50 mm and a depth 40 mm, are drilled into the top of the cylinder. One cavity is placed in the middle of the phantom and the other is centered between the first cavity and the edge of the phantom. Measurements can therefore be made in the center or the periphery of the phantom. Peripheral measurements are important because radiologic CBCT examinations target structures located peripherally on the human head. The bottom of the phantom receives 15 holes, each 1 mm in diameter and 5 mm deep, with a distance of exactly 10 mm between the holes, and with the holes drilled in 2 perpendicular lines. Figure 1 shows a photograph of the phantom, and Figure 2 presents drawings of the main body of the phantom.

Two cylindrical inserts 50 mm in diameter and 50 mm tall were manufactured to fit the phantom; one of solid Plexiglas and the other with four 10-mm-diameter

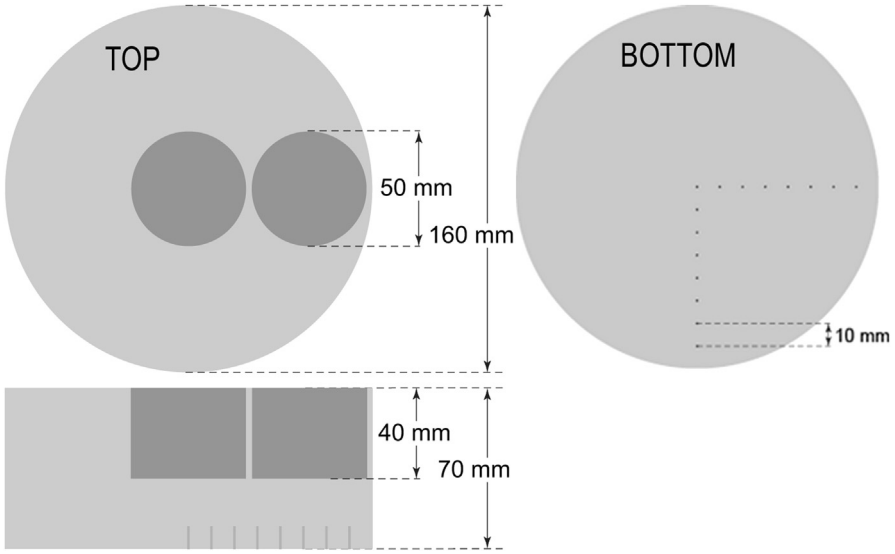

Fig. 2. Drawing of the main body of the phantom.

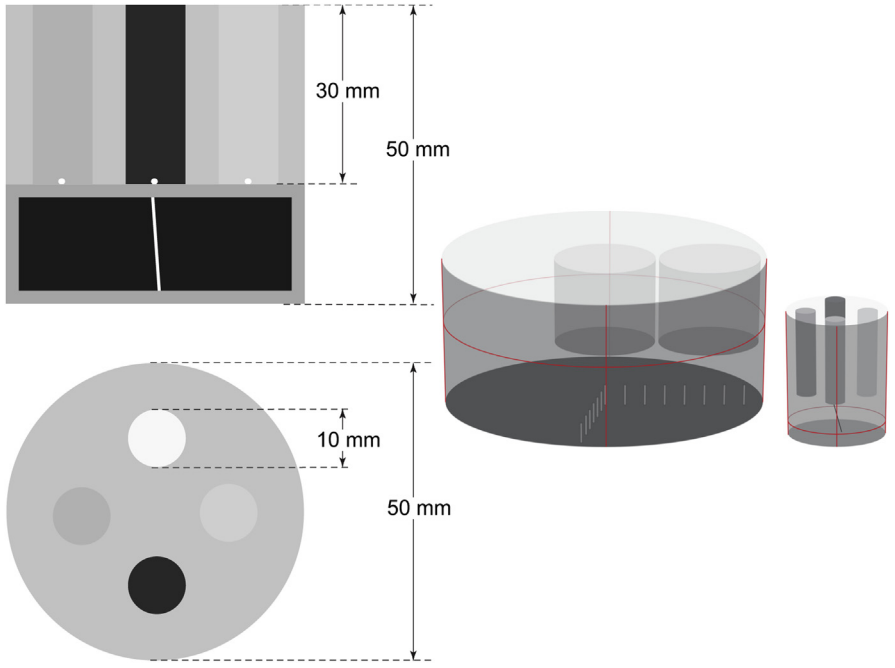

Fig. 3. Drawing of the insert containing objects for parts of the image quality assurance procedures.

holes drilled to a depth of 30 mm. The centers of these holes describe the vertices of a square with 18-mm sides (25.5-mm diagonal). Rods of polyethene, nylon, acetal, and polytetrafluoroethylene (Teflon) are inserted into these holes. At the bottom of each rod, a 0.3 mm tantalum bead is placed into a small hole drilled exactly in the center of the rod. The bottom 20 mm of the insert is hollow and contains a 0.1-mm-diameter stainless steel wire, mounted in such a way that the direction of the wire will never coincide with any of the principal coordinate planes, regardless of how the insert is rotated. Correct positioning of phantoms in any CT or CBCT scanner is crucial for making reproducible measurements.[5-7] As a positioning aid, thin grooves have been milled into the phantom surface. The main body is marked with a horizontal line around the perimeter at a depth of 30 mm from the top and with 4 vertical lines at a 90° angle. The density insert is marked correspondingly with a line around the perimeter 10 mm from the bottom and 4 vertical lines.

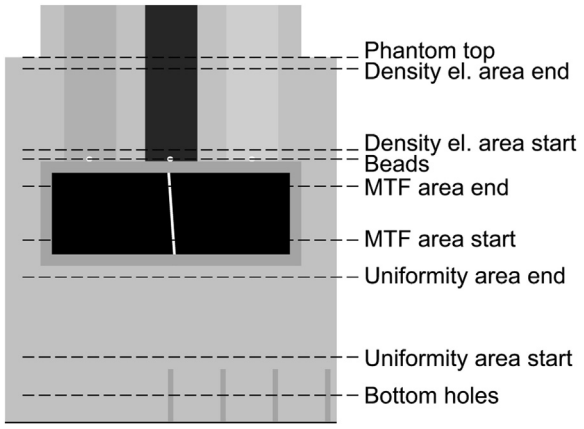

Fig. 4. Side projection of an enlarged part of the phantom with its different sections. (*MTF*, modulation transfer function.)

Figure 3 shows drawings of the insert and the position of the milled grooves.

The design of the insert enables gathering measurements of all of the aforementioned IQA parameters with a single scan, even for the smallest fields of view (40 mm diameter × 40 mm height). Figure 4 shows a projection image of the phantom with labels indicating the various sections.

Images are exported from the modality as axial (XY-plane) images in DICOM format (Digital Imaging and Communications in Medicine) with the thinnest slice thickness available. Thin slices are important for measurement of a properly oversampled point spread function.

Software environment

Software for transforming the methods and algorithms described in this article can be developed using many different environments (e.g., Matlab, IDL, ImageJ). We chose to develop the software as a plugin (extension) to the image processing and analysis package ImageJ.[8] The plugin was programmed in the Java programming language. Images must be in DICOM format to be processed. User input is limited to (a) loading the image stack containing the axial images of the phantom and (b) scrolling to the slice containing the beads in the bottom of the inserted plastic rods. Complete analysis is thereafter performed automatically, and the software generates a report with tables and diagrams as a PDF document. All data are also exported to a comma-separated text file that can easily be imported into third-party software for further analysis and long-term follow-up.

Description of methods and software analysis

Low-contrast resolution. This method is based on Albert Rose's principle, proposed in 1948,[9-12] regarding detectability of threshold signals in electronic systems that register photon events, such as television cameras. For single-photon events, Rose states that a signal that deviates by 2 SDs has a probability of 0.023 of being a noise fluctuation rather than a true, detectable threshold signal. The probability for signals deviating by 3 SDs is 0.0013.

For a 2-dimensional image of a homogeneous object (flat-field image), the SD in Rose's case corresponds to the SD of the mean value for a large number of circular regions of interest (ROIs) of a certain size placed in the central 10% (area) of the slice. The slice used for this evaluation is chosen from the area called "Uniformity area" in Figure 4. The number of ROIs that our software examines is 1000 for a specified ROI size. The ROIs are randomly placed with their centers inside the central 10% area of the slice and are allowed to overlap. The mean pixel value in each ROI is measured, and after completion the SD of the mean values is calculated. The threshold value for low-contrast detectability is set to 3 times the SD. This practically eliminates the possibility that a deviating signal is due to random variation. By repeating this procedure with 10 different ROI sizes, where ROI size number n will produce an ROI with a diameter of 2 $n^{1.5}$ pixels, the software can create a contrast-detail diagram.[13] Part of this procedure is illustrated in Figure 5. This objective method for producing a contrast-detail diagram has been recommended by the Swedish Radiation Safety Authority for determining the low-contrast detectability of medical CT scanners since 1995.[14]

The area under the contrast-detail curve can be used as an index to monitor the low-contrast properties of the CBCT unit over time. Also, the sum of the mean pixel values for the 10 ROI sizes, which is equal to the signal response from the CBCT unit when exposed at a certain voltage (kV) and electric charge (mA s), produces a value that reflects the reproducibility and sensitivity of the system.

Uniformity. In the same flat-field image (slice) that is used for low-contrast resolution, 5 ROIs are placed centrally, "north," "east," "south," and "west." The ROI diameter should be approximately 20% of the diameter of the phantom. The peripheral ROIs should not be placed too close to the phantom edge, because this will affect the mean pixel value for those ROIs, owing to the cupping artifact present in all scanners. Effectively, uniformity is measured in the central 75% area of the homogeneous image.

The software calculates the mean value and SDs for the pixel values within the ROIs. It also calculates the integral and differential uniformity values according the method originally proposed by the National Electrical Manufacturers Association (NEMA)[15] for QA of nuclear medicine gamma cameras. Calculating the NEMA indices includes using a 9-point filter, with weightings

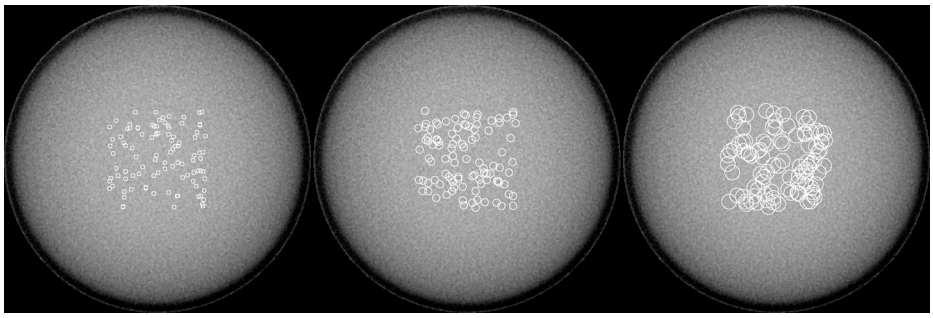

Fig. 5. Example of randomly placed regions of interest of different sizes.

1	2	1
2	4	2
1	2	1

Fig. 6. Nine-point convolution filter for preprocessing of the flat field image before calculating NEMA uniformity indexes. (*NEMA*, National Electrical Manufacturers Association.)

shown as shown in Figure 6. The central 50% area of the homogeneous image, after removing the edge pixels, is smoothed once by convolution with this 9-point filter function. The weighting factor for a pixel outside the analyzed area in the 9-point filter is zero. The smoothed value is normalized by dividing by the sum of nonzero weighting factors. The purpose of this convolution step is to discard pixel value outliers produced by extreme random events or nonstochastic noise such as defect pixels.

NEMA defines the integral uniformity index as:(Eq. 1)

$$\textit{Integral uniformity} = \pm 100 \cdot \frac{(\max - \min)}{(\max + \min)} \quad \text{(Eq. 1)}$$

in which "max" and "min" are the maximum and minimum pixel values in the central 50% of the image area.

The software also calculates the differential uniformity index inside the central 50% of the image area as defined in Equation 1, save that the "max" and "min" values are measured in 5 adjacent pixels in the row (X) and column (Y) directions. Measurements are made for all groups of 5 adjacent pixels in the central 50% of the image, and the largest differences are used to index differential uniformity in the X and Y directions.

Noise power spectrum. The software again uses the central 50% of the same flat-field image (slice) to examine the noise power spectrum (NPS). The NPS is defined as[16]:(Eq. 2)

$$NPS\left(\alpha,\varphi\right) = N_X N_Y \Delta_X \Delta_Y \left\langle \left| FT\{\Delta P(x,y)\}\right|^2 \right\rangle \quad \text{(Eq. 2)}$$

where N_x and N_Y are the number of pixels and Δ_x and Δ_Y are the pixel widths in the X and Y directions, respectively. The term ΔP(x,y) represents the deviation of the pixel value at the coordinate (x,y) from the mean pixel value in the image, and FT $\{\Delta P(x,y)\}$ represents the Fourier transform of the pixel value deviation matrix.

Equation 2 yields a 2-dimensional NPS, which is not easy to perceive. For simplicity, this matrix can be integrated over all phase angles φ to give a 1-dimensional representation:(Eq. 3)

$$NPS_{1D}(\alpha) = \int_0^{2\pi} NPS(\alpha,\varphi)\, d\varphi \quad \text{(Eq. 3)}$$

Pixel number constancy. For this purpose, the software used 2 images (slices): (1) an image of the plastic rods with the beads (the slice called "Beads" in Figure 4) and (2) another without the beads (the bottom drawing in Figure 3). It uses the position of the beads to generate 5 circular ROIs with a diameter of 6 mm; 4 inside the plastic rods and the fifth in the center (Plexiglas). The software calculates mean values and SDs and lists them in ascending order, regardless of the location of the rods (rotation of the phantom insert).

Geometric accuracy. For large fields of view, the software uses the pattern of drilled holes at the bottom of the phantom ("Bottom holes" in Figure 4). For small fields of view, it uses the tantalum beads in the center of the plastic rods. The software locates the holes or beads and calculates their interspacing. Results are given as minimum, maximum, and average values. The average value is used for comparison with the true value.

Spatial resolution. The software calculates the modulation transfer function (MTF) from the point spread function of the 0.1-mm steel wire. It locates the pixel with the maximum value in 3 adjacent slices imaging the wire ("MTF area" in Figure 4). The software then takes the pixels in a 64 × 64-pixel area surrounding the pixel with the maximum value, cuts and pastes them as new images, and adds the 3 images together to produce an oversampled point spread function, because the wire is slightly angled in relation to all principal planes.

The oversampled point spread function is then fitted to a Gaussian curve:(Eq. 4)

$$g(x) = \frac{1}{\sigma\sqrt{2\pi}} e^{\frac{-x^2}{2\sigma^2}} \qquad \text{(Eq. 4)}$$

The oversampled points are displayed together with the fitted Gaussian so that it can be determined whether the fit is adequate.

The fitting procedure produces the parameter σ, and Equation 5 determines MTF[17]:(Eq. 5)

$$MTF(w) = FT[g(x)] = e^{-\frac{w^2 \cdot \sigma^2}{2}} \qquad \text{(Eq. 5)}$$

RESULTS

We tested the methods and software with images from most CBCT manufacturers on the market. The procedure runs smoothly, as long as images are in DICOM format. The results presented here provide an example of the method and software output and include only output data from a single QA session, testing images from 1 particular product from 1 specific manufacturer. The unit used here was a Morita (J. Morita Mfg Corp, Kyoto, Japan) 3D Accuitomo 170 operated at 90 kV, 5 mA, field size 80 × 80 mm, and 360° data acquisition. After setup and alignment of the phantom, acquisition of the data volume, and generation of the image stack, the complete evaluation procedure takes approximately 40 seconds using a standard PC. Figure 7 shows an example of a PDF page generated by the software, to which the following results refer.

Low-contrast resolution

The contrast-detail diagram in the PDF protocol indicates the low-contrast limit for 10 different ROI sizes. The diagram also shows the area under the curve, as well as the cumulative mean value for the 10 ROI sizes ("sensitivity index"). The units for those quantities are strictly [pixel value units × mm] and [pixel value units], but the quantities can be regarded as dimensionless because they are used only for constancy monitoring.

Uniformity

The PDF protocol shows the central and peripheral data together with integral and differential uniformity values according to the NEMA methods.[15]

Noise power spectrum

The PDF protocol shows the NPS. To simplify interpretation, the software integrates the true 2-dimensional NPS over all phase angles into a 1-dimensional representation. The unit for NPS_{min}, NPS_{mean}, and NPS_{max} is strictly [mm^2], but the quantities can be regarded as dimensionless because they are used only for constancy monitoring.

Pixel number constancy

The PDF protocol gives the ROI location and measured values for CT number constancy.

Geometric accuracy

The PDF protocol presents the distance between adjacent holes as minimum, maximum, and mean values.

Spatial resolution

The PDF protocol shows the oversampled point spread function together with the Gaussian fit. This extra precaution ensures that the curve fitting is appropriate. Lastly, the PDF protocol shows the MTF curve based on the fitting.

DISCUSSION

All vendors of dental CBCT units supply phantoms and sometimes software for evaluation of image quality parameters (e.g., for spatial resolution measured as the MTF). However, these phantoms generally do not support measurement of all the crucial IQA parameters. Moreover, the use of the vendor phantoms often requires multiple phantom setups and exposures, and the routines for documentation and long-term follow-up are rudimentary. This does not encourage an unexperienced user, such as a general dental practitioner, to perform IQA on a regular basis. The purpose of this work is to suggest IQA methods that are understandable and easy to use and thus will stimulate the user to perform IQA on a regular basis. Image QA must never be regarded as an imposition; instead, it should be considered a natural part of the imaging routine.

In the era of analog imaging, IQA in medical and dental radiology was entirely based on quality control

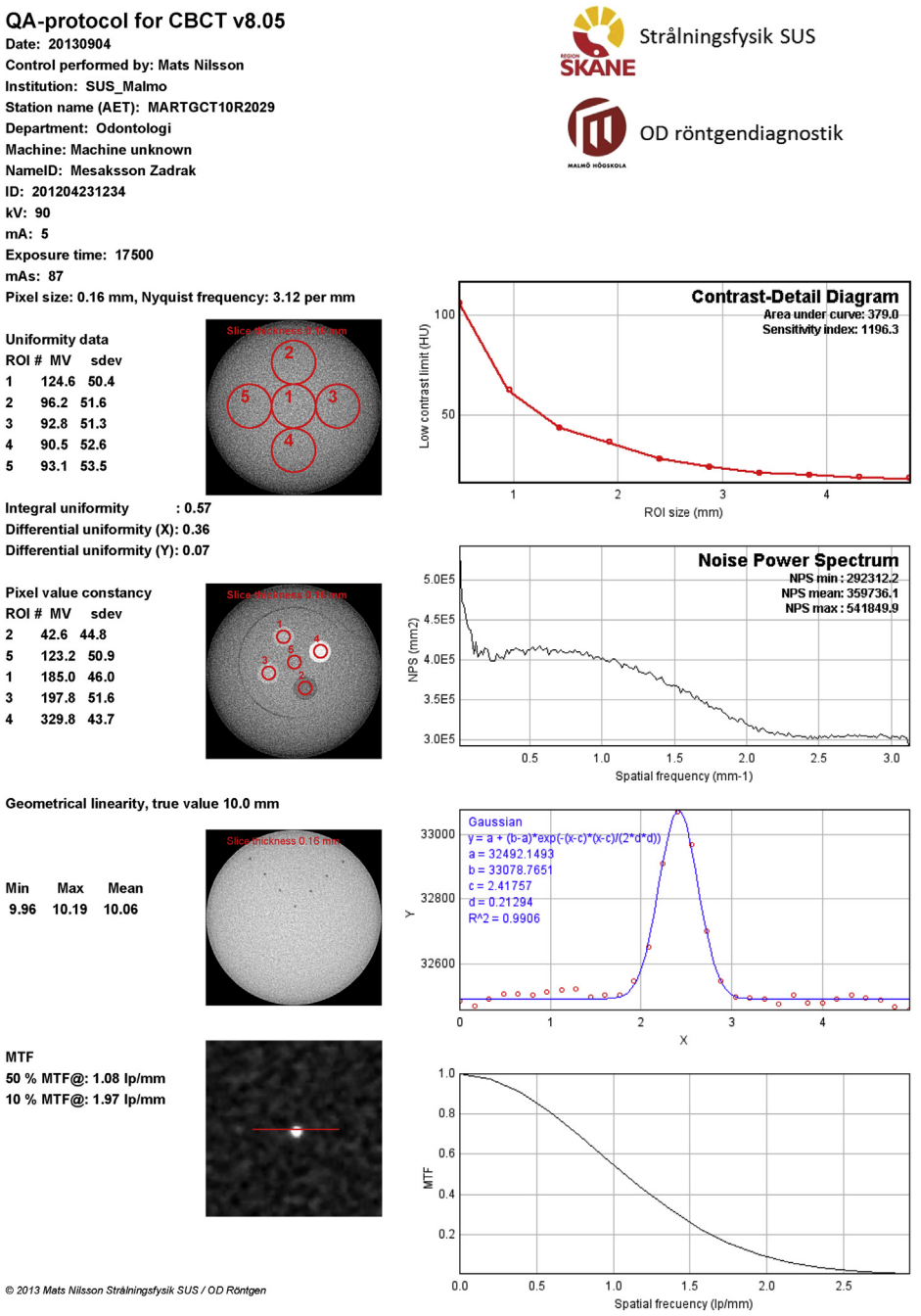

Fig. 7. Software-generated PDF protocol of image quality assurance results.

phantoms containing objects for evaluating properties such as contrast and spatial resolution. The only option for users was to evaluate the QA images subjectively by examining them on a light box and estimating what could or could not be seen. These methods of using the same or similar phantoms has, for whatever reason, survived into the digital era; it is still widely used, which means that IQA is usually still based on subjective evaluation methods.

For digital images, this has an even greater potential for error than it had for analog x-ray film images. Aside from observer variability, the digital environment introduces a number of confounding factors that make subjective IQA very uncertain. Examples of such factors include variability due to:

- Condition, calibration, and settings of the viewing display

- Quality of the graphics card to which the display is connected
- Interaction of the viewing software with the graphics card
- Environmental factors such as reflections on the display screen, the ratio of diffuse/specular light impinging on the display surface, and the ambient light level (illuminance) in the room

QA in digital radiology depends on the devices used to show images. One key issue in the analog era for image quality control was daily sensitometry measurements for monitoring the film development process to ensure a constant film response for a step-wedge image. Today, the quality of the viewing display is just as important as was the quality of film development in the analog era.

A poor graphics card in the computer used to display images can cause strange effects when displaying grayscale images owing to imperfect interpolation algorithms, producing truncation or round-off errors. Also, different viewing programs may display an image differently, even on the same computer using the same graphics card. All these factors clearly illustrate that subjective evaluation of digital images for QA has a high risk of error. Thus, substituting objective methods for subjective techniques is a high priority when determining procedures for medical, as well as for dental, radiology QA. This was the first goal our work sought to achieve. This principal standpoint is shared by the authors of the recently published article on IQA of CBCT machines.[3]

Our second goal in designing QA procedures for dental CBCT was simplicity. For QA methods to reach the growing part of the dental community that uses CBCT, the equipment and software must allow any dentist, dental nurse, or hygienist to successfully carry out the QA procedure, and the results produced must be understandable to the user. We firmly believe that a QA system for dental CBCT designed to be used by physicists and engineers will never be accessible enough to be used by dental personnel in the clinic.

To be simple, QA procedures should also be quick. An IQA procedure that is to be performed weekly or even monthly must not take much time from the dentist's busy patient schedule. If IQA procedures are too time-consuming, dentists will be less likely to perform regular QA. Our goal was that anybody should be able to complete the IQA procedure in less than 10 minutes. It appears that, with training, this can be reduced to approximately 5 minutes.

The third requirement we established was low cost. Existing phantoms are very good, but not easy to use, and their cost makes them unobtainable to most of the dental community. The QA phantom should be as inexpensive as possible while still enabling quantification of the most important key parameters. To keep costs down, the evaluation software should be based on an open-source platform as well.

Uniformity is a key parameter for which a dental CBCT differs substantially from a medical CT. Owing to its acquisition geometry and lack of beam-shaping filters, a dental CBCT unit has poor uniformity performance. This can be seen in Figure 7, where pixel values at the periphery of the homogeneous phantom slices are more than 100 pixel units lower than at the center. The corresponding figure for a medical CT is around 3 to 5 pixel units. This is important to consider when evaluating low-contrast resolution (the contrast-detail diagram). Because of this lack of uniformity, the 1000 ROIs of varying sizes will all need to be placed in a limited area at the center of the image, in the homogeneous part of the phantom. If not placed so, the mean value of the 1000 ROIs will show variation caused by poor uniformity rather than by random variations within a largely homogeneous area. Homogeneity of the phantom is necessary for the validity of Rose's statement.[4-6] For this reason, we chose to analyze an area covering only 10% of the image.

Both geometric accuracy and spatial resolution are sensitive to how the phantom is placed in relation to the voxel matrix produced after reconstruction. Sampling of the distances between the holes drilled with an interspacing of 10 mm works by finding the pixel in each hole with the lowest pixel value. The exact location of this pixel will depend on how the image of the hole is distributed among neighboring voxels, sometimes giving a value slightly higher or lower than 10 mm. The mean value, however, represents geometric accuracy. The same reasoning is used when the small tantalum balls are used, except for that the highest pixel values are searched for. The same applies for sampling of the point spread function. In principle, adding 3 areas of 64×64 pixels, centered on the pixel with the highest pixel value, will always produce an adequately oversampled point spread function. The sampling points, together with the curve fit, are included in the protocol to assure the operator that the MTF curve is generated from valid input data.

The displayed MTF in Figure 7 is calculated in the X direction. Because the thin wire is slightly angled (approximately 7°) to all principal planes, the point spread function will be equally well oversampled in the Y direction and, accordingly, the MTF in the Y direction will be identical to that in the X direction, which has been verified experimentally during the production of this article. Using a thin wire for production of an oversampled point spread function in the Z direction for obvious reasons will be difficult, given that the fan beams in the scanner are acquiring data principally in

the XY plane, which would produce strange and varying images of the wire in the Z direction. The alternative of using sharp edges of dense materials and using oversampling of derivatives of the edge spread functions produced will introduce a sampling artifact owing to beam hardening, so that was never considered as an alternative. The approach by Steiding et al.,[3] who use an aluminum sphere to sample the edge spread functions in the X, Y, and Z directions, also involves beam hardening artifacts, which are accordingly discussed in their article. To keep to this article's principle of simplified IQA, we settled for a spatial resolution measurement in only 1 dimension. As a constancy check for spatial resolution in simplified IQA, it is certainly sufficient.

CONCLUSION

We consider the phantom and methods presented in this article to be a step toward engaging clinical dental personnel to undertake regular QA testing with CBCT units. The equipment and evaluation software produce objective measures, and they are easy to use and affordable. Presently, we are further developing the software to eliminate all user interaction with the program, so that it can automatically find and process the images/slices that contain the structures necessary for analysis.

REFERENCES

1. European Commission. Radiation Protection No. 172 Cone Beam CT For Dental And Maxillofacial Radiology. Evidence-Based Guidelines. Directorate-General for Energy, Directorate D — Nuclear Energy, Unit D4 — Radiation Protection. 2012. ISSN: 1681-6803.
2. Holroyd JR, Walker A. *Recommendations for the Design of X-ray Facilities and the Quality Assurance of Dental Cone Beam CT (Computed Tomography) Systems*. Chilton, Didcot, Oxfordshire, England: Health Protection Agency, Centre for Radiation, Chemical and Environmental Hazards, Radiation Protection Division; 2010:ISBN: 978-0-85951-664-8.
3. Steiding C, Kolditz D, Kalender WA. A quality assurance framework for the fully automated and objective evaluation of image quality in cone-beam computed tomography. *Med Phys*. 2014;41:031901. http://dx.doi.org/10.1118/1.4863507.
4. Baek J, Pelc NJ. Local and global 3D noise power spectrum in cone-beam CT system with FDK reconstruction. *Med Phys*. 2011;38:2122-2131.
5. Oliveira ML, Tosoni GM, Lindsey DH, Mendoza K, Tetradis S, Mallya SM. Influence of anatomical location on CT numbers in cone beam computed tomography. *Oral Surg Oral Med Oral Pathol Oral Radiol*. 2013;115:558-564. http://dx.doi.org/10.1016/j.oooo.2013.01.021.
6. Mah P, Reeves TE, McDavid WD. Deriving Hounsfield units using grey levels in cone beam computed tomography. *Dentomaxillofac Radiol*. 2010;39:323-335. http://dx.doi.org/10.1259/dmfr/19603304.
7. Molteni R. Prospects and challenges of rendering tissue density in Hounsfield units for cone beam computed tomography. *Oral Surg Oral Med Oral Pathol Oral Radiol*. 2013;116:105-119. http://dx.doi.org/10.1016/j.oooo.2013.04.013.
8. Rasband WS. ImageJ. U.S. National Institutes of Health, Bethesda, Maryland, USA, 1997-2012. Available at: http://imagej.nih.gov/ij/. Accessed January 2, 2014.
9. Rose A. Television camera tubes and the problem of vision. In: *Advances in Electronics and Electron Physics*. Vol 1. New York, NY: Academic Press; 1948:131-166.
10. Rose A. Quantum effects in human vision. In: *Advances in Biological and Medical Physics*. Vol 5. New York, NY: Academic Press; 1957:211-242.
11. Rose A. *Vision: Human and Electronic*. New York, NY: Plenum Press; 1973. ISBN: 0-306-30732-4.
12. Burgess AE. The Rose model, revisited. *J Opt Soc Am A Opt Image Sci Vis*. 1999;16:633-646.
13. Bushberg JT, Seibert JA, Leidholdt EM Jr, Boone JM. *The Essential Physics of Medical Imaging*. Philadelphia, PA: Lippincott Williams & Wilkins; 2002:287.
14. SSMFS 2008:42. Strålsäkerhetsmyndighetens allmänna råd om prestandaspecifikationer vid upphandling av utrustning för röntgendiagnostik [in Swedish]. *[Swedish Radiation Safety Authority Recommendations on Performance Specifications for Equipment used in Diagnostic Radiology]*. ISSN: 2000-0987.
15. National Electrical Manufacturers Association. *NEMA Standards Publication NU 1-2007: Performance Measurements of Gamma Cameras*. Rosslyn, VA: NEMA; 2007.
16. Dobbins JT III. Image quality metrics for digital systems. In: Beutel J, Kundel HI, van Metter RL, eds. Handbook of Medical Imaging. Vol. 1: Physics and Psychophysics. Bellingham, WA: SPIE Press; 2000:161-222.
17. Derpanis KG. *Fourier transform of the Gaussian*; 2005. Available at: http://www.cse.yorku.ca/~kosta/CompVis_Notes/fourier_transform_Gaussian.pdf. Accessed January 2, 2014.

Reprint requests:

Mats Nilsson, PhD
Department of Radiation Physics
Skåne University Hospital
SE-205 02 Malmö
Sweden
Mats.l.nilsson@skane.se